A stochastic approach to modelling and understanding hillslope runoff connectivity dynamics

Daryl Janzen [a,*], Jeffrey J. McDonnell [a,b,c]

[a] Global Institute for Water Security, University of Saskatchewan, Saskatoon, Canada
[b] School of Geosciences, University of Aberdeen, Aberdeen, Scotland, UK
[c] Dept. of Forest Engineering, Resources and Management, Oregon State University, Corvallis, OR, USA

ABSTRACT

Runoff generation at the hillslope scale is an important component of the hydrological cycle. Recent work has shown that a common hillslope runoff response mechanism is driven by connectivity of saturated patches in the subsurface (via filling and spilling) to a threshold initiation of lateral flow at the hillslope base. Here, we show that directed percolation theory is able to represent this key runoff process including the details of dynamical flowpath development and filling and spilling processes at the soil-bedrock interface. We then use the directed percolation model to investigate how changes in slope angle, soil depth, and subsurface microtopography influence stormflow response. We map the evolving subsurface flow network under different hillslope classes and compare them to the natural system response. Our results suggest that the natural system sheds water more efficiently than randomly generated systems providing some insights into key hydrogeomorphic controls on water shedding in the environment.

© 2014 Elsevier B.V. All rights reserved.

1. Introduction

The mechanisms by which hillslopes store and release water affect many ecological processes through biogeochemical and nutrient cycling (Stieglitz et al., 2003). There is a developing consensus that filling and spilling of infiltrated rainfall at a soil-bedrock interface or along other subsurface impeding layer(s) is a dominant process leading to hillslope runoff in a variety of hydrological systems (Spence, 2010; McDonnell, 2013). Connectivity of saturated patches in the subsurface via filling and spilling leads to threshold flow activation at the hillslope base, and associated material transfer (McGlynn and McDonnell, 2003).

While several new quantitative measures of connectivity have been developed for hillslopes and catchments (e.g. Western et al., 2001; Reaney et al., 2006; Bracken and Croke, 2007; Ali and Roy, 2009), spatially explicit modelling of the connectivity and dis-connectivity that dynamically occurs at a confining layer in the subsurface has proved very challenging. Traditional Darcy-Richards solvers have been used (Ebel et al., 2008; Hopp and McDonnell, 2009; James et al., 2010) but are very computationally expensive and limit the scenarios that can be explored. Simpler

conceptual models have been used (e.g. Weiler and McDonnell, 2003; Tromp-van Meerveld and Weiler, 2008) but they still require more site information (antecedent soil moisture profiles, hydraulic parameters, etc.) than is often available. More problematic is the inherent stochastic nature of fill and spill, connectivity and threshold response—something that defies both physically based and conceptual modelling approaches.

One approach that shows considerable promise for capturing the dynamics of lateral connectivity-associated thresholds is percolation theory. Lehmann et al. (2007) showed that with a small set of simple rules they could match observed threshold response and runoff ratio when modelling subsurface stormflow at the hillslope scale. In other words, percolation theory subsumed the considerable process complexity that is usually described deterministically, linking a stochastic pattern of spatial connectivity with the lateral outflow behaviour.

While useful and certainly a step forward, the traditional percolation theory approach of Lehmann et al. (2007) was perhaps too abstract a stochastic modelling approach because it did not account for the spatial distribution of subsurface topography and soil depth—two key controls on subsurface stormflow dynamics that we have known about since Hewlett and Hibbert (1967). Recent physics-based modelling work (Tromp-van Meerveld and Weiler, 2008) shows how critically important such information is for prediction. The question now is: how can we use a stochastic approach like percolation theory, which is both parsimonious and

* Corresponding author. Tel.: +1 306 966 1558; fax: +1 306 966 1193.
E-mail addresses: daryl.janzen@usask.ca (D. Janzen),
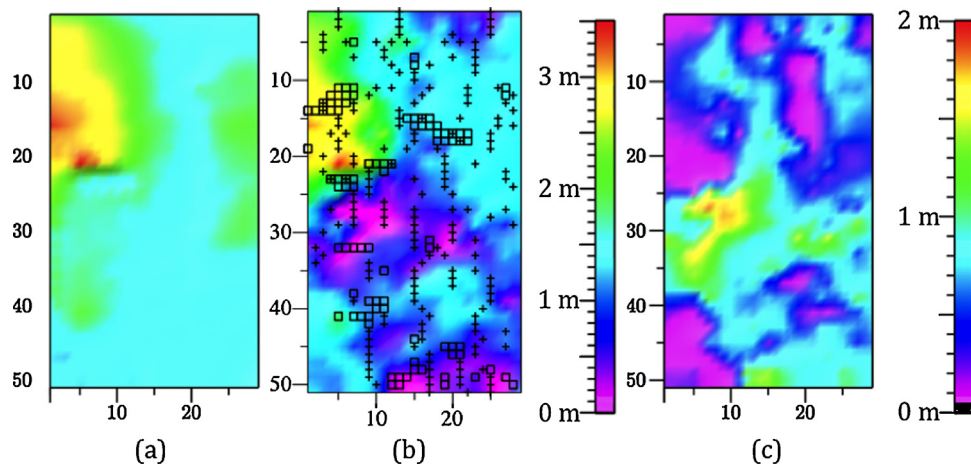jeffrey.mcdonnell@usask.ca (J.J. McDonnell).

Fig. 1. Panola experimental hillslope physical characteristics, with the average hillslope angle, 13.1°, relaxed in order to generate a map of topographic relief. The top of the hillslope is at the top of the figure. The three plots show (a) surface relief, (b) bedrock relief, and (c) soil thickness, in metres over the 29 m × 51 m hillslope section. In (b), cells which are lower than their downslope neighbour are highlighted with squares, and cells which are lower than their left and right neighbours are highlighted with crosses—so it is readily apparent where water following the global gradient will typically pool along ridges, and also which preferential spillways will be taken.

inherently suited to capture the observed linkage between subsurface saturation connectivity and runoff threshold that we aim to describe, but more directly incorporate features that are known to be of critical importance, such as topography and soil depth distribution?

Here we apply the principles of directed percolation to bring process realism into a stochastic, pattern-focused modelling approach for gaining new insights into the dynamics of hillslope connectivity and threshold response, using it as the basis for a description of the movement of water along a subsurface confining layer. Directed percolation theory is a special case, first posed by Broadbent and Hammersley (1957), in which a direction of flow is prescribed at each bond between neighbouring cells on a grid. The advantage of directed percolation is that the direction of flow can be based on the topography of the flow layer (in our case, the topography of the soil-bedrock interface), allowing for more realistic representations of spatial connectivity. Indeed, in accounting for this detail we shall be able to describe naturally connecting flowpaths along heterogeneous surfaces where local gradients do not always follow the global gradient (cf. Fig. 1b), much as Ambegaokar et al. (1971), and particularly Pollak (1972), did in the original papers which used percolation theory to describe electrical conduction within random resistor networks exhibiting similar heterogeneity.

While directed percolation has previously been considered in descriptions of infiltration-excess runoff on rough surfaces (Davy et al., 2001), we are unaware of any previous application to the problem of modelling subsurface stormflow in hillslopes where runoff occurs at a confining layer beneath highly permeable soil, where the non-uniform delivery of water through heterogeneous soil exceeds the infiltration capacity of the lower (e.g. fractured bedrock) layer. In this case, the spatial variability of soil depth adds a significant layer of complexity to the dynamical process of infiltration-excess fill-and-spill at the impeding surface.

This paper outlines how a model based on directed percolation can be used to represent what we call "essential hillslope realism" (following Dietrich et al., 2003), thereby bridging the gap between the abstract statistical realism of modelling approaches like that of Lehmann et al. (2007), which incorporate little detail of the real world, and the detailed realism that process-deterministic approaches are unable to achieve (e.g. due to CPU and resolution limits). Our objectives are: (i) to examine the ability of directed percolation to match observed fill, spill, connectivity, threshold dynamics for a well-characterised hillslope, (ii) to use the model as

a virtual experiment tool (following Weiler and McDonnell, 2003) to explore the effects of slope angle on fill and spill, connectivity and threshold response, and (iii) to examine the effects of soil depth and subsurface topography on connectivity dynamics via the virtual experiment approach.

2. Background on the Panola hillslope

In order to realistically capture the observed process of perched stormflow along soil-mantled bedrock, we develop our directed percolation approach based on field-measured runoff dynamics at the Panola experimental hillslope, located within the Panola Mountain Research Watershed near Atlanta, Georgia, USA. Fig. 1 shows the bedrock and surface relief at Panola along with a map of soil depth. The hillslope angle is 13.1°, with a trench dug at its base (at the bottom of Fig. 1) in order to capture runoff, as described in Tromp-van Meerveld and McDonnell (2006a) and Tromp-van Meerveld et al. (2008).

During storm events which are typically of long duration and low intensity, rain infiltrates vertically into thin (~0–2 m) sandy-loam soil that varies in depth, and therefore reaches storage capacity at different times across the hillslope. When the soil's storage threshold has been reached, water begins filling depressions along the bedrock surface, and eventually spills laterally downslope (cf. the organisation of rills and spillways along the bedrock surface in Fig. 1b, as described in the figure's caption), all while a percentage infiltrates further into the bedrock (Tromp-van Meerveld and McDonnell, 2006a,b). Tromp-van Meerveld et al. (2007) measured a 91% bedrock infiltration loss rate on the Panola hillslope in a series of sprinkling experiments.

The main factor that limits whether any appreciable flow will be observed at the base of the slope is the cumulative rainfall amount, since a certain volume must always go towards saturating the lower part of the soil profile and filling the bedrock depressions before flow in the trench at the base of the hillslope is observed (Tromp-van Meerveld and McDonnell, 2006a). Given a large enough event to produce stormflow, the main physical controls on the process development are then: antecedent soil moisture deficit, bedrock loss rate and bedrock topography.

The antecedent soil moisture deficit depends on both the soil depth, which varies across the hillslope, and the antecedent soil moisture. Data records from 123 storm events at Panola (as reported by Tromp-van Meerveld and McDonnell, 2006a,b) indicate that the antecedent soil moisture does not exceed ~0.41 vol/vol,
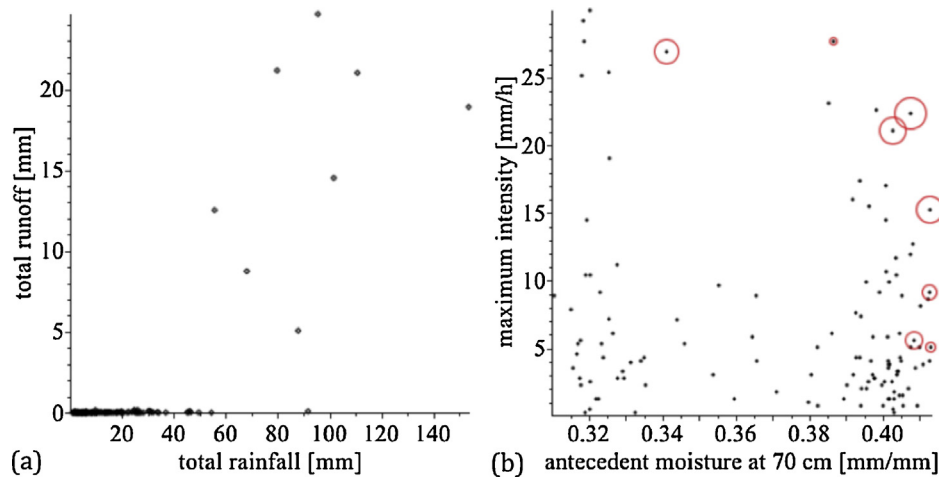
Fig. 2. (a) Runoff as a function of total precipitation, and (b) relationship between antecedent soil moisture and peak hourly averaged rainfall intensity, for 123 events recorded at Panola hillslope. In (b), the total runoff measured at each event is indicated by the radius of a surrounding circle.

and that the majority of significant runoff events occurred when the soil moisture was near this value prior to the storm. Fig. 2b shows how runoff is a complex tradeoff between antecedent wetness, rainfall intensity, and rainfall amounts, whereby low antecedent soil moisture can only produce runoff if peak rainfall intensity or cumulative precipitation is high. The bedrock loss that occurs once soil storage capacity is reached depends on the ratio between bedrock and soil infiltration potential.

In addition to antecedent soil moisture deficit and bedrock loss rate, the other dominant physical control on the runoff generation process at Panola is bedrock topography. Of course, this factor does not vary from one event to the next: water that is delivered vertically through the soil to the bedrock (that does not leak further into it the bedrock) will flow along the bedrock gradient (McDonnell et al., 1996).

3. Methods

3.1. Directed percolation model

We use directed percolation theory to capture the system-governing processes described above. Using a gridded map of the hillslope, the potential for cell i to become saturated is defined as the ratio of the average soil moisture deficit to the moisture deficit at cell i:

$$w_i = \frac{\text{SMD} \cdot \bar{\sigma} + \delta}{\text{SMD} \cdot \sigma_i + \delta},$$

where SMD is the soil moisture deficit, σ_i is the cell's soil depth, $\bar{\sigma}$ is the average soil depth over the hillslope, and δ is the micro-depressional storage capacity at the soil-bedrock interface, which we set equal to 1 mm. Our approach then involves several simplifying assumptions. The most significant of these (only possible in a stochastic model that can be run a number of times) is that the development of a perched water table (i.e. soil saturation development) is binary: a cell in a two-dimensional grid representing the soil-bedrock interface, is simply wet or dry, which we keep track of in a two-dimensional array of 1s and 0s. As we progress through a Monte Carlo simulation (described in more detail below), these 1s and 0s are redistributed as a result of the processes captured by the model, and with enough realisations that the average hillslope saturation levels off, that average is taken to represent the typical evolving saturation pattern during an event with the prescribed conditions and model parameter values. This assumption enables us to simulate complex subsurface flowpath

development within a dynamical and highly heterogeneous system, with little computational expense.

Another significant simplifying assumption made in this analysis is that the antecedent soil moisture deficit and the bedrock loss rates are constant. It would not be difficult to model spatial heterogeneity or time-dependence in either parameter, which the model would handle in much the same way as it does the delivery of rain through spatially heterogeneous and increasingly saturated soil (described below). However, we decided that this further level of complexity would not significantly add to the overall process understanding we have hoped to derive from this virtual tool, because: (i) while there is a two-orders-of-magnitude variation in soil depth values, the soil moisture, e.g. tends to vary by only a factor of 2 (determined from publically available data published by Tromp-van Meerveld et al., 2008), so the greater contribution to spatial variation in SMD should come from the variation in soil depth rather than the variation in soil moisture; (ii) soil moisture content is likely correlated with soil depth, with shallower soils drying more readily, which would serve to homogenise soil moisture deficit to some extent—but in our model the same effect can be achieved by decreasing the value of SMD, and we emphasise that our purpose, in Section 4.1, is only to constrain *behavioural* model parameters to use in our subsequent analysis; and (iii) there is equifinality between the effects of the two constant parameters (see e.g. Fig. 4a below), so modelling detailed spatial variation in them would confound the results anyway. Notwithstanding, use of constant parameter values results in the development of already highly complex subsurface saturation patterns as shown below.

Before we begin running Monte Carlo simulations that add rain to the hillslope, we take account of the principal heterogeneities in soil depth and topography by constructing two arrays with the same length and width as the hillslope. In one, the gradients in the directions of each point's four nearest neighbours[1] are ranked in

---

[1] We also used an eight-directional scheme, which resulted in slightly greater runoff, earlier threshold, etc., given the same conditions. However, the effect was found to be equivalent to that of slightly lowering the loss rate or antecedent moisture deficit—i.e., there is equifinality in our model between the precision of the routing mechanism and the values of the other model parameters—so we chose to present only the results obtained with the four-directional scheme. There is no great loss of information in this since, as noted, there is already equifinality between the two model parameters. However, it is interesting to note that increasing from a four- to an eight-directional scheme (a topological change) is effectively similar to decreasing the bedrock loss rate or the antecedent soil moisture deficit (i.e. our two dimensionless physical parameters)—as each tends to increase connectivity.

order from lowest to highest using the topographic map. A second array is then constructed with the discrete values of the initial probability density function for rainwater to be delivered through the soil to the bedrock (the "delivery PDF"). This delivery PDF is found by normalising the array of w_i's defined above so that they sum to 1.

It should be noted that while δ is technically another model parameter that could be varied, the added complexity of allowing it to do so does not actually increase model versatility: if δ is much larger than SMD $\cdot \sigma_i$, the unnormalised weights $w_i \approx \delta/\delta = 1$, and if it is much smaller than SMD $\cdot \sigma_i$, the soil moisture deficit SMD cancels from $w_i \approx (\text{SMD} \cdot \bar{\sigma})/(\text{SMD} \cdot \sigma_i)$—therefore, SMD is rendered ineffective either way; on the other hand, the model behaviour at these two extremes is precisely what is intended to be captured by considering soil moisture deficit—i.e., when SMD is very small, and only a little water is needed to saturate the soil anywhere, the weights level off so that the delivery PDF becomes more uniform; and as SMD becomes larger, the heterogeneity of the delivery PDF *should* become as pronounced as that of the soil depths. Therefore, it is really only interesting to vary SMD between these two extremes, which we can do effectively by holding δ constant. Furthermore, if δ were 0, the weights w_i would be infinite at cells where the bedrock is exposed ($\sigma_i = 0$), whereas even exposed bedrock should hold about a millimetre of rain in micro-topographic depressions—so we have taken that as the value of δ.

Next, given our array of ranked gradients and the initial delivery PDF, we begin simulating cumulative subsurface stormflow development during a rain event. In each iteration of these Monte Carlo simulations, a cell is randomly selected using the delivery PDF and if it was not previously selected (as in the first iteration) it becomes saturated. The soil depth is set to zero as a way of setting the soil moisture deficit to zero for the now-saturated cell and the delivery PDF is updated accordingly. A two-dimensional "saturation map" array (that initially contains all 0s) is given a 1 at that cell's location to indicate the presence of perched water at the soil-bedrock interface.

While we saturate a particular cell with a particular moisture deficit value in each Monte Carlo iteration, the depth of water that is infiltrated is always calculated as the average moisture deficit over the hillslope; therefore, the depth of water that would saturate the entire hillslope, divided by the hillslope area, is added to a single cell at each iteration. This assumption is intended to allow the routing and saturation development processes to be captured stochastically, and is relevant only in the calculation of cumulative rainfall and (in case water is routed laterally down to the trench) runoff. We will justify this significant simplifying assumption with some remarks after describing the routing algorithm.

In subsequent iterations, when a previously saturated cell is selected, we first use a maze-solver on the saturation map to determine the extent of the locally saturated area within the hillslope (which may be only the one cell that was selected, or a locally connected pond or ribbon; we will refer to this generally as the "local patch"[2]). The water that falls on the saturated cell is then routed down to the lowest unsaturated neighbour at the perimeter of the local patch. In this step, a number of points are taken into consideration:

i. We assume that water can flow freely between adjacent cells that are both saturated (site percolation).
ii. The excess water that has been delivered through a previously saturated cell eventually spills along the gradient to the lowest dry cell adjacent to the local patch. This is a "directed" percolation model in which the spill direction is *dynamically* determined—i.e., the same governing rules always apply, but the spill direction at a given cell may change from one iteration to the next depending on the evolving saturation pattern.
iii. In some cases water will not flow along the gradient from the particular cell that was selected—e.g., if the cell in that direction was not previously saturated—but will preferentially take a connected path, in accordance with percolation theory, only to follow the gradient at the bottom where the excess water from the wet patch must spill.
iv. For the same reason, water will tend to work its way out of a depression, along the slope of shallowest ascent—which is the slope of steepest descent in the case that all directions from the local patch point uphill.
v. When water does eventually spill laterally, saturating the lowest dry neighbour of the local patch, the soil column at that cell should *not* become saturated, so the delivery PDF is *not* updated. Thus, we model lateral subsurface stormflow beneath soil that may not yet be saturated all the way through, but occurs as a result of thinner soil upslope.
vi. Iterations of the model *are not* time steps: only subsequent iterations affecting the same local patch can be considered as subsequent in real time, whereas iterations with no causal connection could be in any order.
vii. Water only makes its way to the outlet (trench) through connected flowpaths that develop dynamically in this way; but by the time a connected path to the outlet has formed, the hillslope tends to be saturated enough that water often lands somewhere along it, and measurable runoff occurs. Indeed, such connectivity-related thresholds are a fundamental feature of percolation theory, which is the primary reason for considering the subsurface stormflow generation process in this way.

The routing step is the main step in the model algorithm. When it is complete, the final step of an iteration is to account for leakage into the bedrock. This is done at a pre-defined random fraction of iterations, by locating the *highest* point in the locally connected patch, and replacing the 1 at that location in the saturation map with a 0. The idea is that in the course of an iteration where leakage occurs, the full volume of water delivered to a saturated patch eventually gets redistributed along the gradient at the bottom of the local patch, as usual. However, as this occurs, the same volume of water will leak into the bedrock throughout the patch, allowing the water in the uppermost cell to drain into the lower cells where some storage opened up through bedrock leakage. The fraction of iterations where this occurs is the bedrock loss rate.

Lastly, it is important that the number of iterations be large enough for the sample that is drawn from the dynamically evolving delivery PDF to be statistically valid. We ran typically about 10^4 iterations in an event that added 100 mm of water over an area containing approximately 1500 cells, which we then deemed sufficient when the products are averaged over 25 model realisations (see Section 4.1).

3.2. Model implementation

Our aim is to use the directed percolation model as a virtual tool that will help us to explore the effects to runoff generation processes at the hillslope scale when soil depths and topography are changed. Also, since we are interested in capturing the cumulative outflow and also the emergence and dynamical evolution of

---

[2] The locally saturated area, or "local patch", therefore represents the two-dimensional extent in which a connected shallow water table is supposed to exist at the soil-bedrock interface. The area may be as small as a single cell, but may variably extend outwards along "ribbons" where runon has occurred, or could be a larger pond. In the percolation literature, such "local patches" are typically referred to as "clusters"—but as we mean here to describe the presence of liquid water rather than an aggregate of discrete cells, the word "patch" more closely resembles the various two-dimensional forms we might expect there to be in reality.

the flow network at the soil-bedrock interface, we require some means of assessing that. We therefore introduce parameters that are meant to capture the full dynamical extent of saturation, and compare to the delivery PDF. For the purpose of assessing the effects that topography and soil depth have on both cumulative outflow and the dynamical extent of hydraulic activity at the subsurface, we investigated the variation in six output parameters that are intended to broadly characterise the system:

   i. *cumulative runoff* at 100 mm of rainfall;
  ii. rainfall *threshold*, defined as the depth of rain required to produce 1 mm of runoff, which Tromp-van Meerveld and McDonnell (2006a,b) established as the amount associated with hillslope connectivity at Panola;
 iii. average *runoff ratio*, calculated directly from i. and ii., i.e.

$$\frac{\text{cumulative runoff} - 1\,\text{mm}}{100\;\text{mm} - \text{threshold}};$$

  iv. *saturation frequency*, calculated as the spatially and temporally averaged frequency during a 100 mm event, that a water table exists at the soil-bedrock interface—i.e., the spatial and temporal frequency of saturation at the flow surface;
   v. a variant of *flowpath depth* (cf. Asano and Uchida, 2012), defined as the temporally averaged saturation frequency at each point, multiplied by the soil depth there, then averaged over the entire surface; and
  vi. *delivery halflength*, which we define as the upslope distance within which 50% of the water should be delivered to the bedrock; e.g., the delivery halflength calculated from the Panola soil depth map is 0.57, which means that the soil is thinner on the upper half of the slope, so half of the rainwater that finds its way to the soil-bedrock interface, which can potentially contribute to runoff, should be in the upper forty-three percent.

These six measures of hydraulic activity are intended to capture when a hillslope will shed water (ii.), how efficient it will be in doing so when that occurs (i. and iii.), and the extent of subsurface saturation during a storm event (iv.) in relation to where water is most likely to be delivered to the subsurface (vi.) and how much is routed to where it is less likely to have come through the soil matrix (v.).

While the reasons for considering parameters i.–iv. and vi. are obvious—e.g., we are interested to see what effects the changes in delivery pattern will have on runoff characteristics, such as whether the rainfall threshold (ii.) is positively correlated with delivery halflength (vi.), as one might expect[3]—the relevance of v. is further explained now. The usual measure of flowpath depth is defined as the volume of water that passes through each point, multiplied by soil depth, and is intended as a proxy for transit time since greater values of the latter should result when water emerges at the bedrock through deeper soil, or when it passes underneath thick soil having been fed by points upslope where the soil is thinner (Asano and Uchida, 2012). In fact, the very existence of a water table below deep soil should indicate the same, so that our variant of flowpath depth should be as useful. Furthermore, we note that this variant would be more accessible to field measurement, as it is possible to remotely measure and record the water level inside a network of capped wells with high frequency.

---

[3] In fact, our results indicate that threshold is only loosely correlated with delivery halflength.

4. Results and discussion

4.1. Ability of directed percolation to represent measured patterns and response

The effects of randomisation in our directed percolation model caused the dynamical system to evolve somewhat differently in each realisation. So, by construction, our directed percolation model did not produce the same outputs each time it ran with a given set of inputs. System-governing rules were imposed so that the flowpath development was *similar* from event to event. The first step of our calibration was therefore to determine how many realisations of the model should be necessary before the average values of our characteristic parameters levelled off. This was done using two different sets of parameters, chosen arbitrarily to represent dry (SMD = 0.15) and wet (SMD = 0.02) initial moisture conditions (cf. Fig. 2b: measured antecedent soil moisture values range from ~0.31 to 0.41 vol/vol; therefore, these soil moisture deficit values should represent realistic limits). Bedrock loss rates (0.4 and 0.9, respectively) were then chosen so that the threshold would be roughly as observed at Panola by Tromp-van Meerveld and McDonnell (2006a).

Fig. 3a shows the cumulative fraction of cells sampled as the number of realisations increases from 1 to 50, and Fig. 3b-f shows the variation in the average value of each parameter over the same range of realisations. Note that when SMD = 0.02, cells with soil depth less than 0.1 m/0.02 = 5 m should become saturated in a 100 mm rainfall event, and when SMD = 0.15, cells with soil depth less than 0.67 m should become saturated in a 100 mm event. In the former case, all cells should become saturated since the maximum soil depth on the Panola hillslope is 1.87 m, whereas only 58% of our soil depths fit the latter constraint. The fact that less of the hillslope should be sampled in the latter case is reflected in Fig. 3a; however, the model is clearly undersampling in both cases (in one realisation, 90% of the cells are sampled when SMD = 0.02, rather than 100%; and 38%, rather than 58%, are sampled when SMD = 0.15), so we compensate for this by considering average outputs from a number of realisations. Given the uncertainty in the average values from each of these sets of realisations (estimated as the sample standard deviation), we decided that all the averages levelled off by 25 realisations in both the wet and dry cases.

Having found the number of realisations necessary to determine typical average outputs from a storm event with given antecedent soil moisture deficit and bedrock loss rate, the next step was to determine the values of these parameters that should represent typical conditions for an event at Panola where runoff would occur. We emphasise that the purpose of this analysis was not to determine "the" values of antecedent soil moisture deficit and bedrock loss rate at Panola, as these are variable parameters—i.e., as Fig. 2b shows, the average antecedent soil moisture varies by a factor of at least 0.1 vol/vol; and indeed, we expect the bedrock loss rate to vary depending on rainfall intensity and soil moisture conditions, so that e.g., if rainfall intensity peaks when the soil is already mostly saturated and a water table is present throughout much of the hillslope, a greater portion of that rain should run off, and the loss rate would therefore be less. The fact that a given amount of precipitation does not translate to a well-defined amount of runoff is evident from Fig. 2a, where the rainfall-runoff data do not fall along a well-defined curve. This scatter occurs *because of* factors like antecedent moisture and rainfall intensity, which vary from event to event—and indeed, Lehmann et al. (2007) found it useful to separate the observational data into events with "wet" and "dry" antecedent soil moisture conditions. Our objective here was not to account for this scatter and determine actual values of the antecedent soil moisture deficit and bedrock loss rates for each individual event, or even for broad classes of events. While
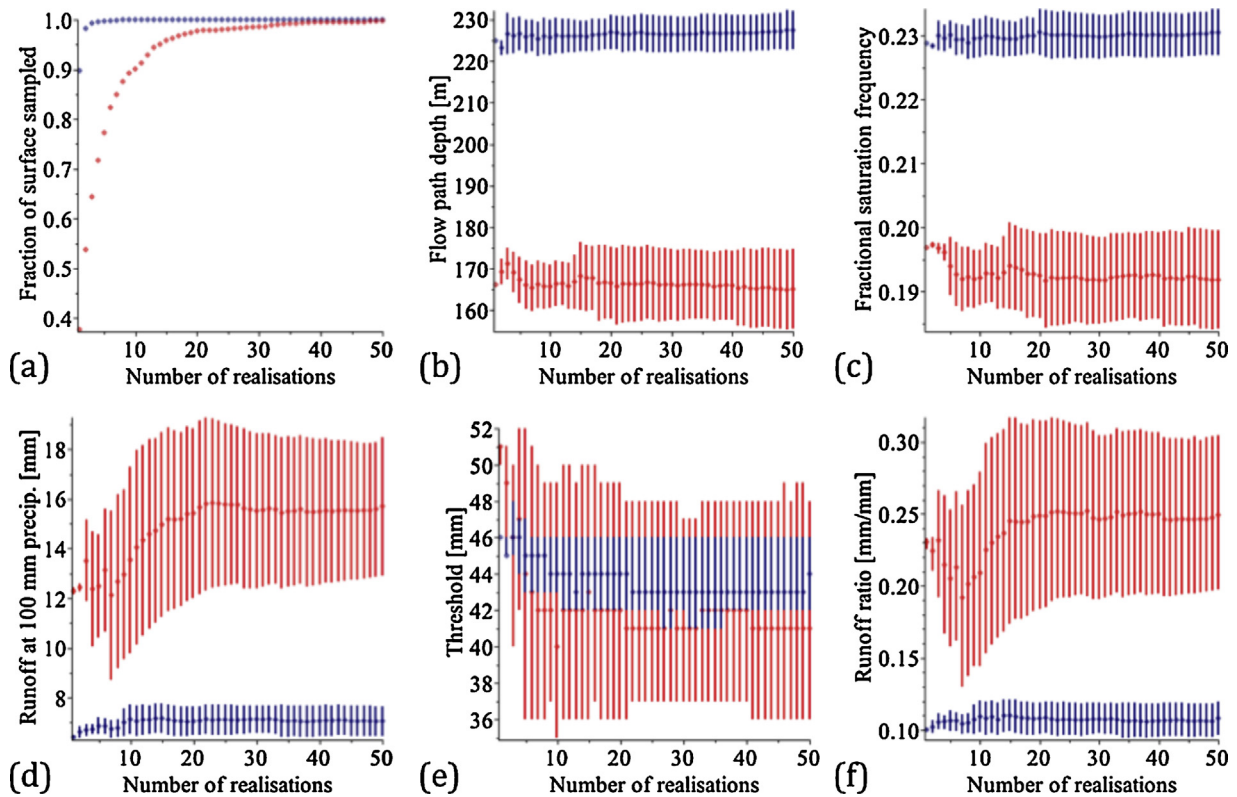
Fig. 3. (a) Cumulative fraction of surface sampled, and (b–f) variation in different characteristic parameters, as they are averaged over the number of model realisations, with uncertainty calculated as the sample standard deviation. In (b–f), the values when antecedent moisture deficit is low (SMD = 0.02, shown in blue) and high (SMD = 0.15, shown in red) both level off by 25 realisations. Loss rates of 0.9 for low SMD and 0.4 for high SMD were chosen so that the threshold would be roughly as observed at the Panola hillslope. (For interpretation of the references to colour in this figure legend, the reader is referred to the web version of this article.)

interesting, this approach has already been successfully explored (e.g., Lehmann et al., 2007; Tromp-van Meerveld and Weiler, 2008), so another iteration with a different model is not likely to significantly impact our understanding. Instead, our approach has been to utilise broad characteristics in the observables—viz. the roughly 50 mm rainfall threshold (Fig. 2a), and the fact that most runoff-producing events occurred under already wet conditions, when the antecedent soil moisture was near its maximum (Fig. 2b)—in constraining behavioural model parameters that represent realistic average conditions at the Panola hillslope. For, having accomplished this, we will subsequently hold these values constant as we vary other physical characteristics of the hillslope and investigate the outcomes of doing so, in Sections 4.2 and 4.3.

In order to determine appropriate behavioural model parameters, we ran the model on a grid of parameter values, with antecedent moisture deficits ranging from 0.01 to 0.20, by 0.01, and loss rates ranging from 0.00 to 0.95, by 0.05. From this grid of results, we constrained a primary set of behavioural parameters by first requiring the uncertainty in their rainfall threshold (for producing at least 1 mm of trenchflow, as per Tromp-van Meerveld and McDonnell, 2006a) to fall within the 45–55 mm precipitation input range.

Fig. 4a is a contour graph (with contour lines drawn at 10 mm increments) of cumulative runoff at 100 mm of precipitation, modelled on a grid of parameter values with the sub-range of behavioural parameters displayed as red and blue dots. The black x's on this graph show parameter values that resulted in significant runoff before 45 mm of precipitation, and the white x's indicate the range of parameters where there was no significant runoff even after 55 mm of precipitation. The black region in Fig. 4a above the white x's shows events with less than 1 mm of runoff at 100 mm of precipitation.

The red and blue dots in Fig. 4a indicate a wedge in parameter space through which higher moisture deficits are compensated by decreased loss rates, and vice versa, to produce an appropriate runoff threshold. Furthermore, the contour graph indicates that the cumulative runoff, along with the threshold, is similar for all events within this wedge. This is shown more clearly in the complementary cumulative rainfall-runoff plot in Fig. 4b, onto which the observational data from Fig. 2a have been superimposed. The overlapping uncertainty bounds displayed there with the same colour-coding, were determined from the standard deviation in runoff throughout each set of 25 realisations.

Fig. 4b shows the measured Panola data plotted against the modelled range. Indeed, the majority of observations—aside from those which obviously fall outside our 45–55 mm rainfall threshold specification (such as a 91.7 mm event in which only 0.1 mm of trenchflow was observed, or an event which already had 12.5 mm of trenchflow with only 55.6 mm of rainfall) all fell within the limits defined by the larger red set. This larger wedge in parameter space was further constrained to only the events with wet initial conditions (shown in blue in Fig. 4a and b), up to a maximum antecedent moisture deficit of 0.07. Finally, from this set we chose the median antecedent soil moisture deficit and loss rate parameters, 0.06 and 0.7, respectively, for subsequent use in our analysis.

4.2. The effects of varying hillslope angle on runoff characteristics

Following our initial model calibration, we began the virtual experiments by increasing and decreasing the slope angle of the Panola hillslope while holding parameter values and all other process controls constant. The threshold and cumulative runoff values we obtained as functions of hillslope angle ϕ, indicate that the real hillslope (at an angle of 13.1°) sheds water more efficiently
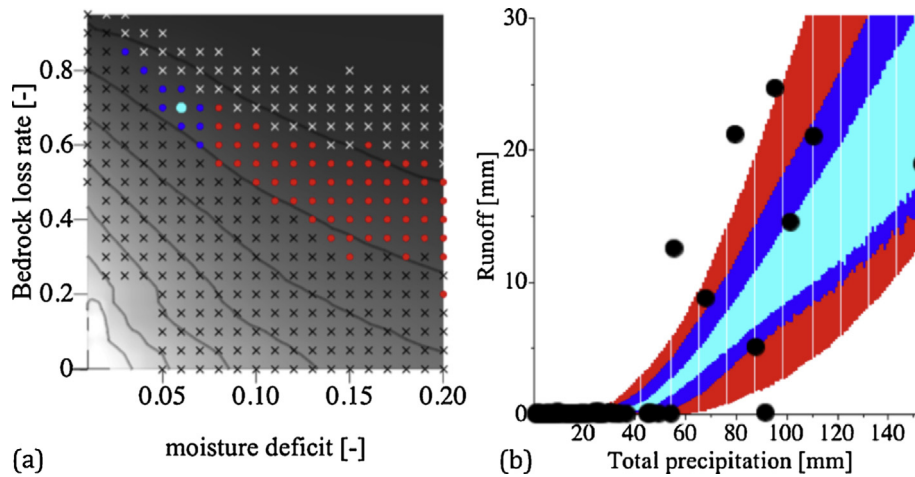
Fig. 4. (a) Runoff at 100 mm precipitation is shown by contours at intervals of 10 mm over the parameter range modelled; and (b) runoff as a function of precipitation for behavioural models with threshold uncertainties in the 45–55 mm range, compared with observational data from Fig. 2a. Behavioural model outputs and parameters are shown in red, along with a blue subset of low antecedent moisture deficit realisations, and finally the median parameter set, used in our subsequent analysis, is shown in cyan. Parameters marked by a black x produced runoff too early, and those with a white x produced more than 1 mm of runoff only after 55 mm. (For interpretation of the references to colour in this figure legend, the reader is referred to the web version of this article.)
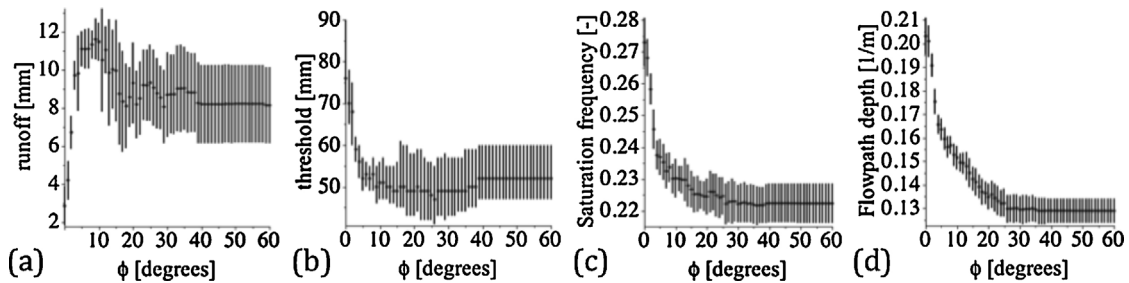

Fig. 5. Variation of (a) cumulative runoff at 100 mm of precipitation, (b) rainfall threshold, (c) saturation frequency, and (b) flowpath depth, with changing hillslope angle ϕ for Panola. There is a peak in the amount of runoff (a), along with a threshold minimum (b), corresponding roughly to the real hillslope angle of 13.1°, while saturation frequency and flowpath depth monotonically decrease with increasing ϕ. Runoff ratio has the same form as cumulative runoff, and is therefore not displayed; and delivery halflength, which depends only on the soil depth map, is constant at 0.57.
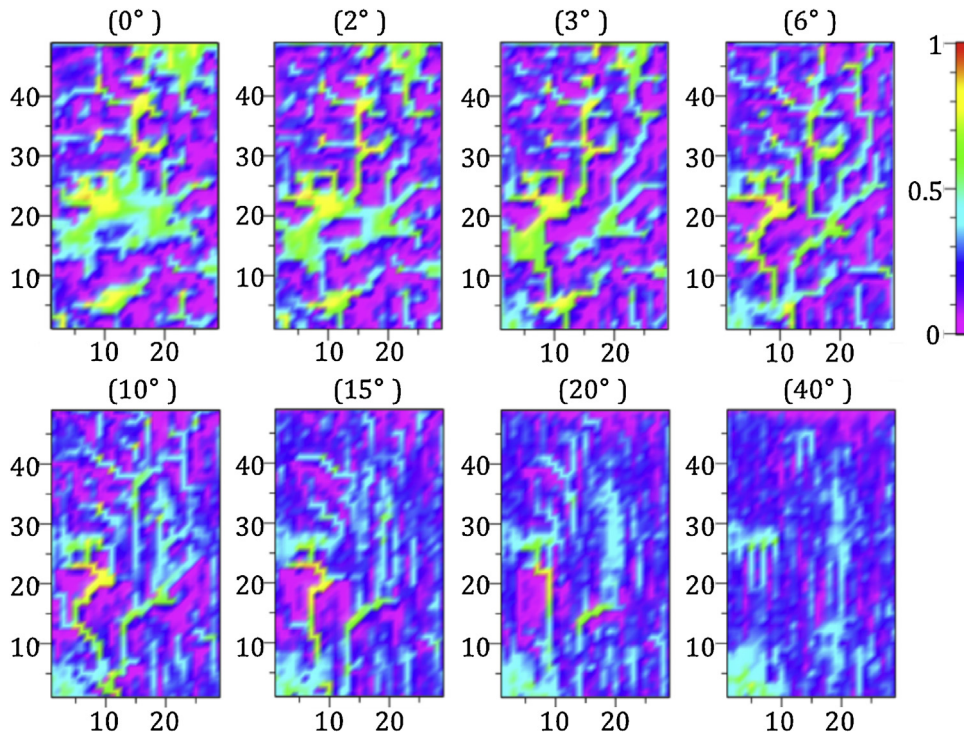

Fig. 6. Maps of fractional saturation frequency across the hillslope (dimensions in metres), averaged over the course of 100 mm precipitation events for model realisations at rotated hillslope angles (as indicated above each plot).
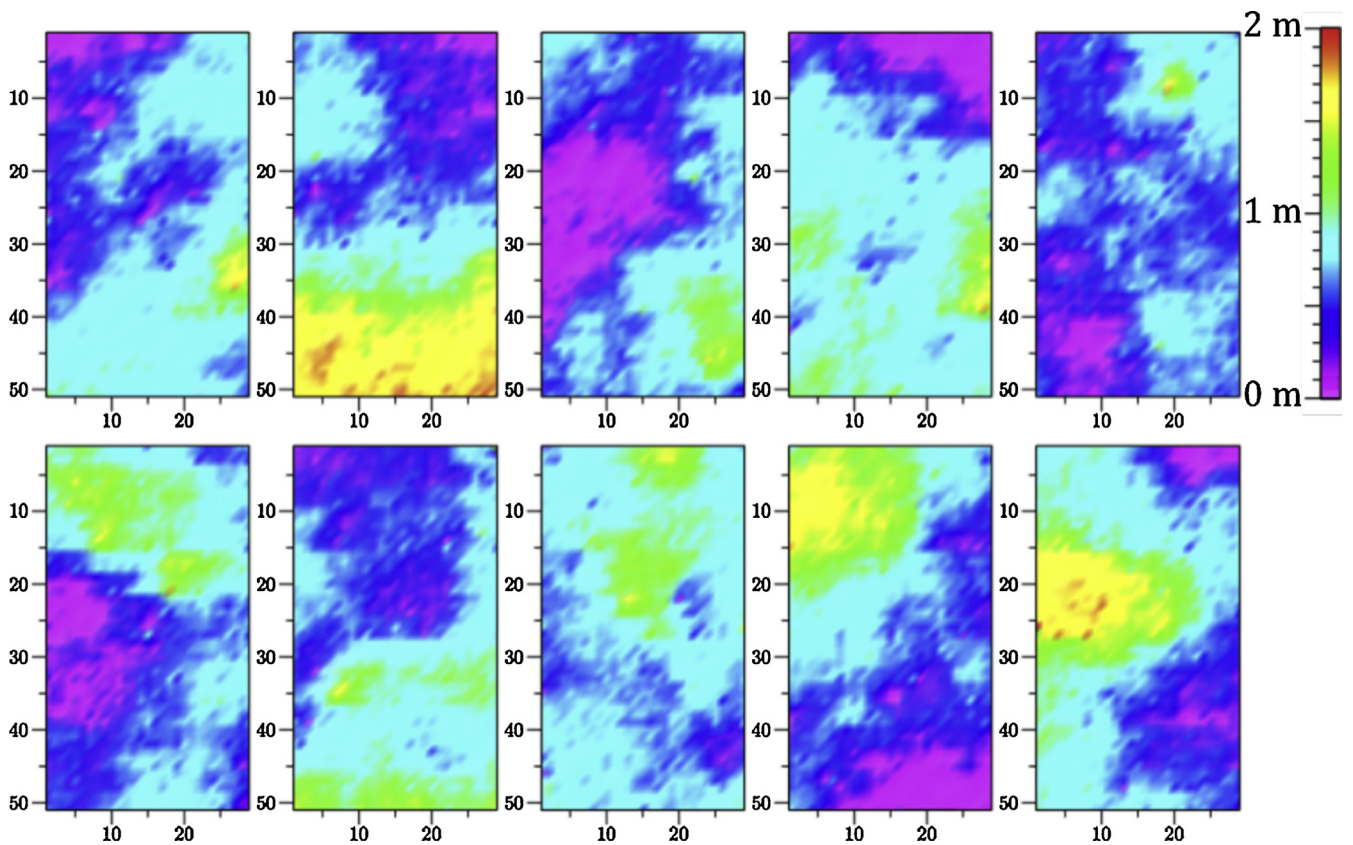
Fig. 7. Ten of the 100 soil depth maps used in investigating the effects of changing delivery patterns to the bedrock, as well as changes to the bedrock topography.

than when its slope angle is increased or decreased (Fig. 5). The reason for this is shown by comparing these results to the spatial maps of saturation frequency (Fig. 6). There, it can be seen that when slope angle is very low, water mostly ponds in very large depressions. As the slope is increased these ponded areas decrease in size and the slope becomes increasingly well drained as a dendritic network of major flow lines emerges. If the slope angle is increased further, those major flow lines disappear, as the diagonalised gradients of the natural flow network are eventually erased (at $\phi \gtrsim 40°$) and the gradient at each point is directed straight downhill.

Evidently, it is through these main ribbons of mobile flow that optimise the connectivity of each point on the hillslope to the outlet, that water is most efficiently shed from the hillslope. In contrast, at greater slope angles when the gradient is everywhere directed straight downhill, each column of cells across the hillslope needs to "build its own road" to the outlet, since the water never connects with a major flow line. These findings amplify Hopp and McDonnell's (2009) analysis of four specific slope angles chosen for their physics-based simulations. The present work with our directed percolation model, which could be run at increments of 1°, reveals the inflection points in Fig. 5a and b at $\phi \approx 13°$.

We found a monotonic decrease in saturation frequency with increasing slope angle (Fig. 5c). Fig. 6 explores this further, and shows that at low slope angles, water pools in large depressions. As the slope angle increases, water continues to be diverted along the main flow lines, which remain saturated throughout most of the event and therefore keep the average high. Nevertheless, the saturation frequency does decrease because the diverted water no longer ponds in large depressions, but runs off. When the slope angle is increased even further, the organised, mobile ribbons of flow disappear and the average saturation decreases.

4.3. The effects of varying soil depth and bedrock topography on runoff characteristics

One hundred maps of varying soil depth were generated, all with roughly the same mean (0.63 m) and standard deviation (0.35 m) as the actual Panola hillslope soil map. We used a fractal landscape generator based on the diamond-square algorithm of Fournier et al. (1982) which produced statistically similar overall soil depth patterns, despite having very different localised depth details. To ensure a consistent range of soil depths, we hand-picked nine values from the actual soil depth map and placed them randomly around the grid to act as seeds for the algorithm in each of the hundred realisations. Our algorithm then ran around the rectangular grid much as it does in the original diamond-square algorithm, using the four nearest generated or seed depths in calculating soil depth at each point. We found that a Hurst exponent of 0.8 consistently produced a similar distribution of soil depths, with roughly the same average and standard deviation as the actual soil depth map.

A sample of ten of these maps is shown in Fig. 7. We defined a "delivery halflength" (see earlier discussion in Section 3.2) as the upslope halfway point of the delivery cumulative distribution function (calculated from the delivery PDF). As expected from a random landscape generator, this delivery halflength fit a normal distribution with a mean of 0.5 (Fig. 8).

Since it would be impractical to examine visually the detailed saturation patterns resulting from 100 different delivery patterns (as we did for a sample of rotated hillslopes, in Fig. 6), we attempted to characterise the process through the six parameters discussed in Section 3.2. The variance in these parameters was considered in two separate cases: (i) without changing the actual bedrock topography underneath the soil, so as to assess the effect of changing only the detailed pattern of delivery to the flow layer; and (ii) by subtracting
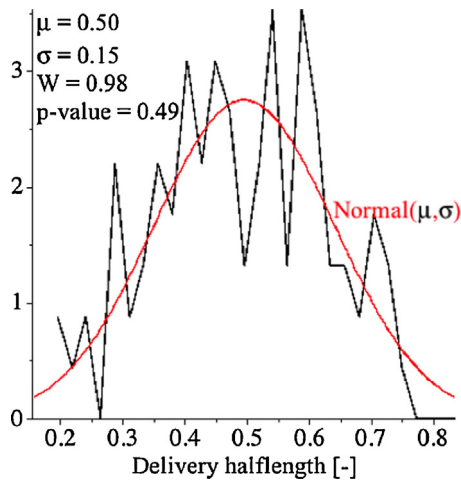
$\mu = 0.50$
$\sigma = 0.15$
$W = 0.98$
p-value = 0.49

Normal(μ, σ)

Delivery halflength [-]

Fig. 8. The delivery halflengths of the 100 randomly generated soil depth maps used in this study are normally distributed about the hillslope's halfway point, with a standard deviation of 0.15. A Shapiro–Wilk test does not rule out the hypothesis that the sample of delivery halflengths is normally distributed.

the soil depth maps from Panola's surface topography, in order to generate a synthetic bedrock topography and compare the results by subtracting them from the results found in the first case. This enabled us to assess the effects of randomly varying the topography in 100 cases where the detailed delivery pattern was the same.

Fig. 9 shows the effects of delivery pattern alteration on all five parameters (graphs a–e) and the effects when bedrock topography was varied (graphs f–j). When the detailed delivery pattern alone was varied, even though the 100 different delivery patterns used were statistically similar overall, we found significant variation in all five parameters. All but the runoff ratio values resembled a normal distribution, with tails extending out as far as 40% from each mean value; e.g., the cumulative runoff from 100 mm precipitation

events ranged from 8 to 17 mm, and the thresholds range from 25 to 55 mm.

Beyond the notable dependence on the specific details of the soil depth distribution, the natural bedrock topography consistently shed more water than the synthetically generated surfaces, regardless of delivery pattern. Only rarely did more water run off of the synthetic flow layers, or with a greater ratio, than what ran off of the flow layer that has been developed naturally.

This result is consistent with what we found by varying the hillslope angle—suggesting that hydrogeomorphic evolution has led to the formation of "water access channels" on the natural bedrock surface that carry water most efficiently from the hillslope. This is evident from the fact that significantly more (normally distributed with mean 1.9 mm and standard deviation 1.3 mm) runoff occurs, and at a significantly greater ratio (normal with mean difference 0.024 and standard deviation 0.018); but also in the fact that the natural bedrock surface is always less saturated, and the flowpath depth (which effectively indicates transit time) is always less, even though the delivery patterns were the same in each of the 100 simulations we ran and compared.

Our results suggest that variations in delivery pattern and bedrock topography *both* significantly influence subsurface flow and runoff characteristics. While we do not know the hydrogeomorphic evolution of the actual bedrock surface, we hypothesise that the existing drainage structure would pre-date the formation of soil (Heimsath et al., 1999) and reflect embryonic drainage evolution of the bare rock surface. Such drainage evolution (with and without soil) is a key topic in network ecohydrology today (Band et al., 2014) and something that perhaps future work with directed percolation could explore.

It is also useful to consider whether there is any significant interaction between our different parameters—such as, e.g., whether more runoff will be produced and threshold will be lower when the delivery halflength is low (so that most of the water is delivered in the bottom half of the hillslope), or whether flowpath depth (which is meant to indicate transit time) is correlated with runoff
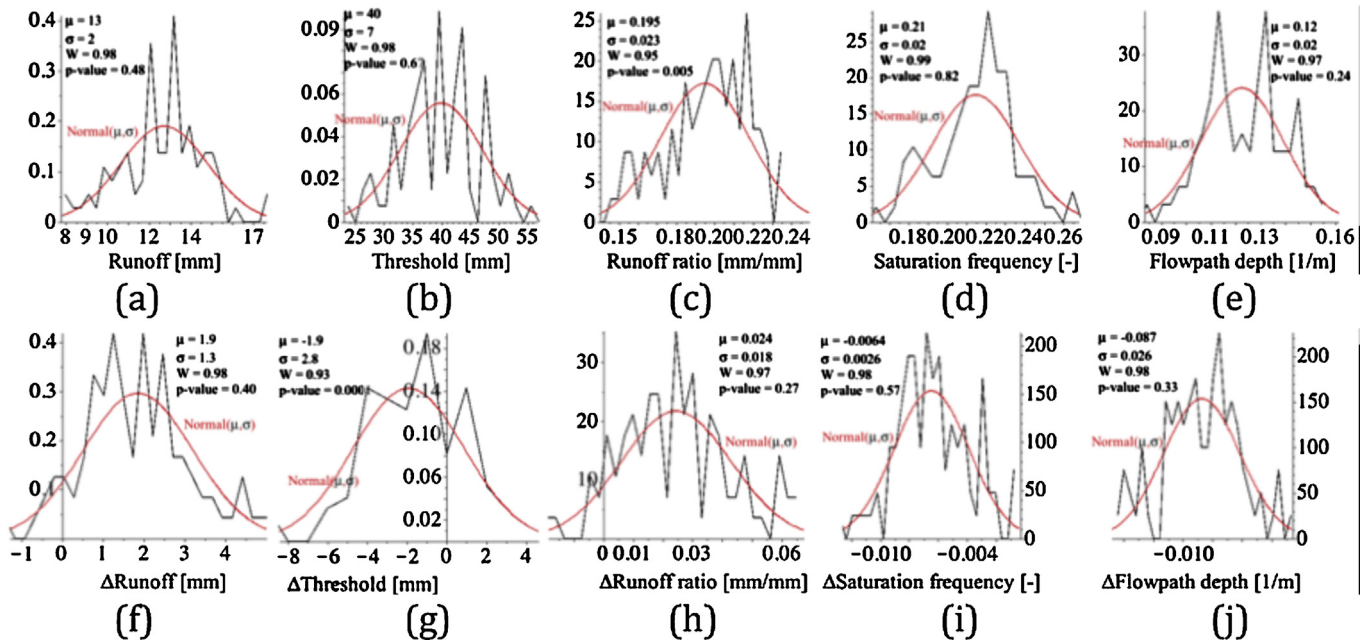

Fig. 9. Variation in the five parameter values for the 100 different soil depth maps used. The graphs in the top row show the frequency distribution of each parameter when the bedrock topography remained unchanged and only the soil depth varied, and the frequency distributions in the bottom row show how each parameter changed when the bedrock topography was changed for each of the 100 delivery patterns. These results indicate both—that changes to the delivery pattern significantly influence the dynamical flowpath development and runoff characteristics (e.g., runoff varied by 9 mm, and threshold by 30 mm, as a result of changing the delivery pattern, even though the general characteristics of the distributions were the same); and that the actual bedrock topography consistently sheds water more efficiently than the synthetic surfaces, regardless of delivery pattern—as there is more cumulative runoff, lower threshold, etc., in the former case.
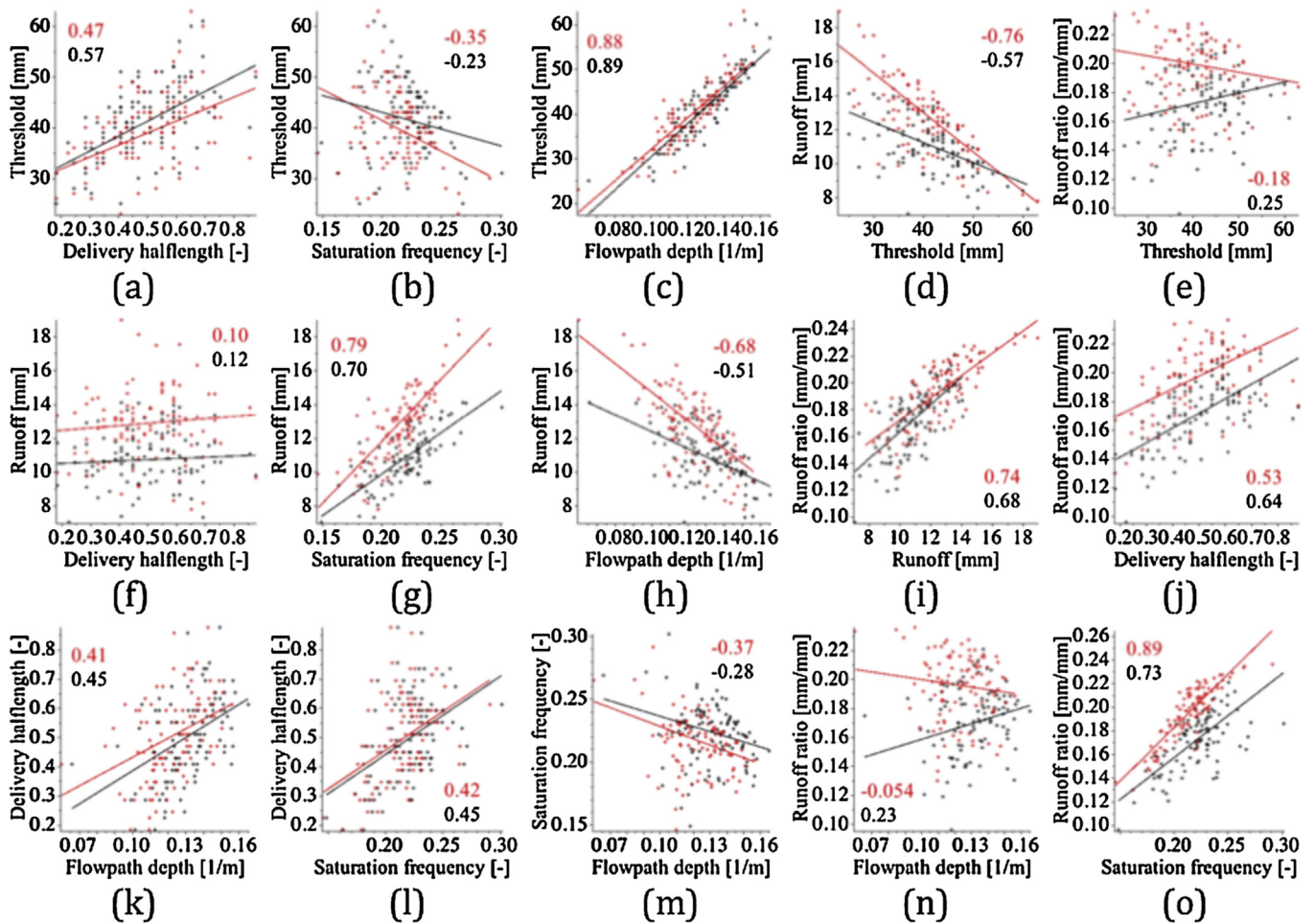
Fig. 10. Fifteen correlation patterns between our six parameters, in the cases where soil is laid on top of the actual Panola bedrock (red) and when the randomly generated soil depth map is subtracted from the Panola surface topography, producing a synthetic flow layer (black). Lines were fit using weights (not shown) depending on the standard deviation in the mean value of each parameter from 25 model realisations, except in the case of delivery halflength, which is a precise fraction of the hillslope length calculated from the soil depth map. The values of Pearson's product–moment correlation coefficient are also shown on each graph. (For interpretation of the references to colour in this figure legend, the reader is referred to the web version of this article.)

threshold. The 15 different correlation patterns between the values of our six parameters are shown in Fig. 10, for both cases (i.e., delivery to both real and synthetic bedrock topographies).

The delivery halflength was weakly correlated with the other five parameters, which is an indication of the complexity of the runoff generation process (e.g., since we might naively have expected a tighter correlation with threshold than there is in Fig. 10a). In fact, it is somewhat surprising that the delivery halflength was not correlated at all with runoff (Fig. 10f); therefore, as much runoff may be generated when the soil is thin at the upper hillslope sections, as when it is thin at the base of the hillslope.

There was significant negative correlation between runoff and threshold, as expected (if runoff begins early, there will typically be more of it in a 100 mm event; see Fig. 10d), as well as significant positive correlation between runoff and runoff ratio (if more runoff was generated, it likely occurred at a greater rate; see Fig. 10i); however, there was no correlation between runoff ratio and threshold (Fig. 10e), so the rate at which water ran off did not depend on when the rainfall threshold was reached.

The strongest measured correlation was between threshold and flowpath depth (Fig. 10c), which was meant to provide an indication of transit time (Asano and Uchida, 2012). Evidently, the requirement for water to percolate laterally through deep soil is a dominant factor on determining when the rainfall threshold will be reached. Indeed, the correlation between these

two parameters is so high that they interact similarly with all others.

Finally, the interactions with saturation frequency (Fig. 10b, g, l, m, o) were peculiar. Saturation frequency was significantly positively correlated with runoff and runoff ratio, so the events that produced the most runoff also had the greatest average spatial saturation over the course of an event. However, the saturation frequency was also consistently greater for delivery to the synthetic surfaces, which we know shed water less efficiently than the natural bedrock topography (cf. Fig. 9f–j, and surrounding text). These seemingly contradictory points were likely due to contrasting effects: greater saturation frequency seems to be associated with the development of major flowlines, or organised flow ribbons that remain saturated throughout the event and skew the average; but topographic inefficiency may lead to the retention of water that does not connect up with a major flow network. The *indication* is that the dynamical system may be too complex to be accurately represented by a single spatial and temporal average—and the implication is that the modeller should be careful not to oversimplify the problem with too much averaging.

5. Summary and future outlook

We were able to reproduce the observed Panola hillslope runoff threshold at 55 mm of cumulative precipitation with directed

percolation theory. Unlike a deterministic approach where we have shown similar capabilities (Hopp and McDonnell, 2009; James et al., 2010), directed percolation is a rules based, ensemble approach that captures the broad process brushstrokes of the highly heterogeneous, dynamically developing flow network throughout the course of a storm event. Such a description is appealing because runoff itself is highly stochastic. For instance, if we examine the saturation patch data for the Panola hillslope as presented by Tromp-van Meerveld and McDonnell (2006b), there is hitherto unrecognised spatial variation in patch saturation locations through a series of progressively larger storms. In other words, the patches that are saturated are not fixed—rather, they appear to have the same overall form, but the detailed pattern changes slightly from event to event.

Our directed percolation approach showed that typical runoff characteristics for the Panola slope corresponded to antecedent soil moisture deficit and loss rates of 0.06 and 0.7, respectively—i.e., we found that in a typical storm at Panola, rain amounting to 6% of the soil's depth would be required before any would percolate through to the bedrock, and 70% would actually be lost to deeper groundwater through further infiltration into the bedrock.

Holding these values constant, we then examined the effects of randomly changing the soil depth map, and therefore the heterogeneous delivery pattern to the lateral flow layer. We found wide variation in the system's response even when these delivery patterns had the same statistical properties. Perhaps more surprisingly, we found that the upslope distance of delivery of rainwater through the soil was correlated only very weakly with the rainfall threshold for runoff generation. It was not correlated at all with the actual amount of runoff that the hillslope would produce. These results indicate that the detailed pattern of delivery of rainwater to the soil-bedrock interface leads to a complex dynamical response that should be accounted for in order to accurately describe and predict runoff at the hillslope scale.

As a complement to our analysis of varying soil depths, we also modelled the effects of changing the bedrock topography, both randomly and simply by altering the slope angle. We found evidence in both cases of evolutionary efficiency in the current branching flow pattern that develops at the hillslope scale. Directed percolation could be a useful tool for examining such hillslope geomorphological processes in future studies.

Acknowledgements

References

Ali, G.V., Roy, A.G., 2009. Revisiting hydrologic sampling strategies for an accurate assessment of hydrologic connectivity in humid temperate systems. Geogr. Compass 3 (1), 350–374.
Ambegaokar, V., Halperin, B.I., Langer, J.S., 1971. Hopping conductivity in disordered systems. Phys. Rev. B 4 (8), 2612.
Asano, Y., Uchida, T., 2012. Flow path depth is the main controller of mean base flow transit times in a mountainous catchment. Water Resour. Res. 48, W03512.
Band, L.E., McDonnell, J.J., Duncan, J.M., Barros, A., Bejan, A., Burt, T., Dietrich, W.E., Emanuel, R., Hwang, T., Katul, G., Kim, Y., McGlynn, B., Miles, B., Porporato, A., Scaife, C., Troch, P.A., 2014. Ecohydrological flow networks in the subsurface. Ecohydrology, http://dx.doi.org/10.1002/eco.1525 (in press).
Bracken, L.J., Croke, J., 2007. The concept of hydrological connectivity and its contribution to understanding runoff dominated geomorphic systems. Hydrol. Process. 21, 1749–1763.
Broadbent, S.R., Hammersley, J.M., 1957. Percolation processes. Math. Proc. Cambr. Philos. Soc. 53, 629–641.
Davy, F., Darboux, F., Gascuel-Odoux, C., Planchon, O., 2001. Which theory for infiltration-excess runoff on rough surfaces? In: Soil structure, water and solute transport = Structure des sols, transfert des eaux et des solutés., pp. 78–80.
Dietrich, W.E., Bellugi, D.G., Sklar, L.S., Stock, J.D., Heimsath, A.M., Roering, J.J., 2003. Geomorphic transport laws for predicting landscape form and dynamics. Pred. Geomorphol., 103–132.
Ebel, B.A., Loague, K., Montgomery, D.R., Dietrich, W.E., 2008. Physics-based continuous simulation of long-term near-surface hydrologic response for the Coos Bay experimental catchment. Water Resour. Res. 44, W07417.
Fournier, A., Fussell, D., Carpenter, L., 1982. Computer rendering of stochastic models. Commun. ACM 25 (6), 371–384.
Heimsath, A.M.E., Dietrich, W., Nishiizumi, K., Finkel, R.C., 1999. Cosmogenic nuclides, topography, and the spatial variation of soil depth. Geomorphology 27 (1), 151–172.
Hewlett, J.D., Hibbert, A.R., 1967. Factors affecting the response of small watersheds to precipitation in humid areas. Forest Hydrol., 275–290.
Hopp, L., McDonnell, J.J., 2009. Connectivity at the hillslope scale: identifying interactions between storm size, bedrock permeability, slope angle and soil depth. J. Hydrol. 376, 378–391.
James, A.L., McDonnell, J.J., Tromp-van Meerveld, I., Peters, N.E., 2010. Gypsies in the palace: experimentalist's view on the use of 3-D physics-based simulation of hillslope hydrological response. Hydrol. Process. 24, 3878–3893.
Lehmann, P., Hinz, C., McGrath, G., Tromp-van Meerveld, H.J., McDonnell, J.J., 2007. Rainfall threshold for hillslope outflow: an emergent property of flow pathway connectivity. Hydrol. Earth Syst. Sci. 11, 1047–1063.
McDonnell, J.J., 2013. Are all runoff processes the same? Hydrol. Process., http://dx.doi.org/10.1002/hyp.10076.
McDonnell, J.J., Freer, J., Hooper, R., Kendall, C., Burns, D., Beven, K., Peters, J., 1996. New method developed for studying flow on hillslopes. EOS Trans. Am. Geophys. Union 77 (47), 465–472.
McGlynn, B.L., McDonnell, J.J., 2003. Role of discrete landscape units in controlling catchment dissolved organic carbon dynamics. Water Resour. Res. 39 (4), 1090.
Pollak, M., 1972. A percolation treatment of dc hopping conduction. J. Non-Cryst. Solids 11 (1), 1–24.
Reaney, S.M., Bracken, L.J., Kirkby, M.J., 2006. Use of the connectivity of runoff model (CRUM) to investigate the influence of storm characteristics on runoff generation and connectivity in semi-arid areas. Hydrol. Process. 21, 894–896.
Spence, C., 2010. A paradigm shift in hydrology: storage thresholds across scales influence catchment runoff generation. Geogr. Compass 4 (7), 819–833.
Stieglitz, M., Shaman, J., McNamara, J., Engel, V., Shanley, J., Kling, G.W., 2003. An approach to understanding hydrologic connectivity on the hillslope and the implications for nutrient transport. Global Biogeochem. Cycles 17 (4), 1105.
Tromp-van Meerveld, H.J., McDonnell, J.J., 2006a. Threshold relations in subsurface stormflow: 1. A 147-storm analysis of the Panola hillslope. Water Resour. Res. 42, W02410.
Tromp-van Meerveld, H.J., McDonnell, J.J., 2006b. Threshold relations in subsurface stormflow: 2. The fill and spill hypothesis. Water Resour. Res. 42, W02411.
Tromp-van Meerveld, H.J., Peters, N.E., McDonnell, J.J., 2007. Effect of bedrock permeability on subsurface stormflow and water balance of a trenched hillslope at the Panola Mountain Research Watershed, Georgia, USA. Hydrol. Process. 21, 750–769.
Tromp-van Meerveld, H.J., James, A.L., McDonnell, J.J., Peters, N.E., 2008. A reference data set of hillslope rainfall-runoff response, Panola Mountain Research Watershed, United States. Water Resour. Res. 44, W06502.
Tromp-van Meerveld, I., Weiler, M., 2008. Hillslope dynamics modeled with increasing complexity. J. Hydrol. 361, 24–40.
Weiler, M., McDonnell, J., 2003. Virtual experiments: a new approach for improving process conceptualization in hillslope hydrology. J. Hydrol. 285, 3–18.
Western, A., Blöschl, G., Grayson, R.B., 2001. Toward capturing hydrologically significant connectivity in spatial patterns. Water Resour. Res. 37 (1), 83–97.